

**SPIN DYNAMICS IN  $\text{La}_{2-x}\text{Sr}_x\text{CuO}_4$   
DOPED WITH Fe: AN ESR-STUDY**

*H.-A. Krug von Nidda<sup>1</sup>, G. Kruschel<sup>2</sup>, A. Loidl<sup>1</sup>, and B. Elschner<sup>2</sup>*

<sup>1</sup>University of Augsburg, 86135 Augsburg, Germany

<sup>2</sup>Technical University of Darmstadt, 64289 Darmstadt, Germany

**СПИНОВАЯ ДИНАМИКА В  $\text{La}_{2-x}\text{Sr}_x\text{CuO}_4$   
С ПРИМЕСНЫМИ ИОНАМИ FE:  
ИССЛЕДОВАНИЯ МЕТОДОМ ЭПР**

*Г.А. Круг фон Нидда<sup>1</sup>, Г. Крушель<sup>2</sup>, А. Лойдл<sup>1</sup>, Б. Элинер<sup>2</sup>*

<sup>1</sup> Университет г. Аугсбурга, Аугсбург, Германия

<sup>2</sup>Тенический университет г. Дармштадта, Дармштадт, Германия



*Volume 6, No. 1,  
pages 155-163, 2004*

<http://mrsej.ksu.ru>

**SPIN DYNAMICS IN La<sub>2-x</sub>Sr<sub>x</sub>CuO<sub>4</sub> DOPED WITH Fe: AN ESR-STUDY**

H.-A. Krug von Nidda<sup>1</sup>, G. Kruschel<sup>2</sup>, A. Loidl<sup>1</sup>, and B. Elschner<sup>2</sup>

<sup>1</sup>*University of Augsburg, 86135 Augsburg, Germany*

<sup>2</sup>*Technical University of Darmstadt, 64289 Darmstadt, Germany*

The electron-spin resonance (ESR) of La<sub>2-x</sub>Sr<sub>x</sub>Cu<sub>1-y</sub>Fe<sub>y</sub>O<sub>4</sub> is investigated on polycrystalline samples for  $0 \leq x \leq 0.3$  and  $0 \leq y \leq 0.1$ . The ESR spectrum consists of the superposition of two Lorentzian lines, which can be unambiguously attributed to Fe<sup>3+</sup> and intrinsic Cu-spin polaron signals. The simultaneous observation of both signals allows to describe the temperature dependence of the relaxation of the Fe<sup>3+</sup> ions in terms of Cu-spin fluctuations.

## 1. Introduction

Since the discovery of high-temperature superconductivity in hole-doped  $\text{La}_2\text{CuO}_4$  by Bednorz and Müller [1], layered cuprates have become a central research field in modern solid-state physics, and an enormous number of experimental and theoretical investigations deals with the correlation of magnetism and superconductivity in these transition-metal oxides [2,3]. Thereby, the dynamic susceptibility of the Cu-spin system plays a key role in understanding the complex physics in cuprates. Besides neutron scattering and nuclear magnetic resonance (NMR), electron-spin resonance (ESR) provides a microscopic probe for the spin dynamics of the electronic system. After a number of early unsuccessful attempts to measure directly the intrinsic ESR signal of the Cu spins in high-temperature superconductors, theoretical analyses derived an estimate for the order of magnitude of the linewidth for the ESR signal of the Cu-spins ( $\Delta H \approx 190$  kOe at 380 K). Due to this large linewidth the Cu resonance could not be detected in conventional ESR experiments [4,5,6]. Nevertheless, intrinsic Cu signals have been detected later on in  $\text{La}_{2-x}\text{Sr}_x\text{CuO}_4$  single crystals and explained by the formation of three-spin magnetic polarons of two Cu spins coupled via a hole spin residing on the bridging oxygen between the Cu ions [7,8]. A related phenomenon is the intrinsic signal from chain fragments in  $\text{YBa}_2\text{Cu}_3\text{O}_{6+\delta}$  single crystals [9,10].

Many ESR experiments have been carried out by doping small amounts of paramagnetic ions, e.g. rare-earth ions like  $\text{Er}^{3+}$  or  $\text{Gd}^{3+}$  on the  $\text{La}^{3+}$  or  $\text{Y}^{3+}$  site or the 3d-ion  $\text{Mn}^{2+}$  on the  $\text{Cu}^{2+}$  site, which indirectly probe the dynamic Cu susceptibility [11]. Detailed ESR investigations by Kochelaev and coworkers have been devoted to the spin dynamics of  $\text{La}_{2-x}\text{Sr}_x\text{CuO}_4$  doped with  $\text{Mn}^{2+}$  ions [12,13]. As a consequence of the relatively strong isotropic superexchange between the Cu and the Mn ions and their nearly coincident Larmor frequencies, the spin systems of the  $\text{Mn}^{2+}$  impurities and the  $\text{Cu}^{2+}$  ions display a collective motion of their total magnetic moments  $M_{\text{Mn}}$  and  $M_{\text{Cu}}$  in an external magnetic field. The relaxation rates between the Mn and the Cu ions are much larger than the relaxation rates to the lattice, and hence the conditions for the well-known "bottleneck" effect are fulfilled (see e.g. Ref. [14]). The lattice includes phonons, charge carriers like oxygen-holes, and spin waves. As a striking sign of the strong bottleneck regime the linewidth is proportional to the inverse Mn concentration, i.e. the higher the Mn-concentration the narrower the ESR line at a fixed temperature.

Here we present ESR results obtained in Fe-doped  $\text{La}_{2-x}\text{Sr}_x\text{Cu}_{1-y}\text{Fe}_y\text{O}_4$ . At first sight, one would expect that the Fe ions behave like the Mn ions with all the consequences which are evidenced in Ref. [12]. But there is an important difference: The fact that we observe ESR spectra even at room temperature shows that one deals with  $\text{Fe}^{3+}$  ( $S = 5/2$ ;  $L = 0$ ). We found that only samples with  $x > 0$  contained dissolved Fe ions. In the  $x = 0$  samples the Fe is clustering and the ESR signal behaves in a peculiar way. This finding is a strong indication that we truly deal with  $\text{Fe}^{3+}$  on a  $\text{Cu}^{2+}$  site and that each  $\text{Fe}^{3+}$  needs at least one  $\text{Sr}^{2+}$  for charge compensation.  $\text{Mn}^{2+}$  has indeed the same electron configuration, hence there is no necessity for charge compensation on a  $\text{Cu}^{2+}$  site.

Several reports exist already about iron ESR in  $\text{La}_{2-x}\text{Sr}_x\text{Cu}_{1-y}\text{Fe}_y\text{O}_4$  [15–22]. These investigations were confined to either the variation of the Sr concentration  $x$  at constant Fe doping  $y$  or the variation of the Fe doping  $y$  for a fixed Sr concentration  $x$ . Usually, a single resonance was detected near  $g = 2$  with a linewidth of the order of 1 kOe, which increases both to high temperatures and low temperatures with a minimum in between. A strong correlation has been found to exist between the temperatures of the minimum in the linewidth and the minimum observed in the electrical resistance [15, 19], suggesting the importance of charge-carrier localization for the low-temperature increase of the linewidth. The high-temperature increase of the linewidth has been discussed controversially in terms of a Korringa process [19] or in terms of Cu-spin fluctuations [17].

The aim of our present work is a comprehensive ESR study of  $\text{La}_{2-x}\text{Sr}_x\text{Cu}_{1-y}\text{Fe}_y\text{O}_4$  dependent on Sr and Fe content in a wide concentration range  $0 \leq x \leq 0.3$  and  $0 \leq y \leq 0.1$ . This enables us to elaborate a systematic dependence of the ESR results on the hole concentration  $p = x - y$  and to show that the Cu-spin fluctuations are the dominant relaxation bath for the Fe-spin.

## 2. Sample Preparation and Characterization

Polycrystalline samples of  $\text{La}_{2-x}\text{Sr}_x\text{Cu}_{1-y}\text{Fe}_y\text{O}_{4-\delta}$  were prepared by solid-state reaction from the oxides  $\text{La}_2\text{O}_3$ ,  $\text{SrCO}_3$ ,  $\text{CuO}$ , and  $\text{Fe}_2\text{O}_3$  in a concentration range  $0 \leq x \leq 0.34$  and  $0 \leq y \leq 0.1$ . Stoichiometric amounts of the starting materials were homogeneously mixed, ground in a mortar, and prereacted in an  $\text{Al}_2\text{O}_3$  crucible at  $950^\circ\text{C}$  in air for 8 hours. Then the material was repeatedly powdered, pressed into pellets, and annealed in oxygen stream at  $1150^\circ\text{C}$  for 40 minutes. The fourth annealing was done for 57 hours and followed by additional 72 hours at  $500^\circ\text{C}$  in oxygen stream. This fourth step was immediately repeated and then the samples were subtracted from the oven. X-ray powder diffraction confirmed the proper  $\text{K}_2\text{NiF}_4$  structure, and additional microprobe analysis revealed a good homogeneity of the samples. The oxygen stoichiometry  $\delta$  was checked in the iron-free samples by means of iodometric titration. As result we found a slight oxygen surplus of  $0 < \delta < 0.02$  for  $x \leq 0.18$  and a deficiency  $-0.03 < \delta < 0$  for  $x \geq 0.2$ . The resistivity of the iron-free samples was found in good agreement with literature data [24], revealing superconductivity for  $0.06 \leq x < 0.33$  with a maximum  $T_c(x = 0.15) \approx 37$  K. Already 2-3% Fe are enough to suppress the superconductivity. The general effect of the Fe substitution on the conductivity is characterized by the fact that trivalent iron annihilates the holes created by divalent strontium. The conductivity at room temperature exhibits a linear decrease on increasing Fe concentration at a given Sr concentration [11]. Comparison of three sets  $x = 0.1, 0.2,$  and  $0.3$  reveals a similar conductivity for the same effective charge-carrier density  $p = x - y$ . Thus the presence of the  $\text{Fe}^{3+}$  impurities has no

additional influence on the scattering of the holes. To explain this, it seems to be reasonable that the additional charge of  $\text{Fe}^{3+}$  with respect to  $\text{Cu}^{2+}$  leads to a strong binding of the electrons in the neighboring oxygen  $p$  orbitals that these orbitals cannot be occupied by holes any more. This hypothesis will be corroborated by the ESR results described below.

### 3. Experimental

The electron-spin resonance (ESR) experiments were performed with a VARIAN E-101 spectrometer working at a microwave frequency of 9.3 GHz. ESR measures the power absorption  $P$  from the transverse magnetic microwave field dependent on the static magnetic field  $H$ . To improve the signal-to-noise ratio the spectra are recorded as the field derivative  $dP/dH$  by lock-in technique with 100 kHz field modulation. The magnetic field was controlled by a temperature-stabilized Hall probe (Bruker). For cooling a continuous-flow He cryostat (Oxford Instruments) was used allowing for temperatures  $4.2 \leq T \leq 300$  K.

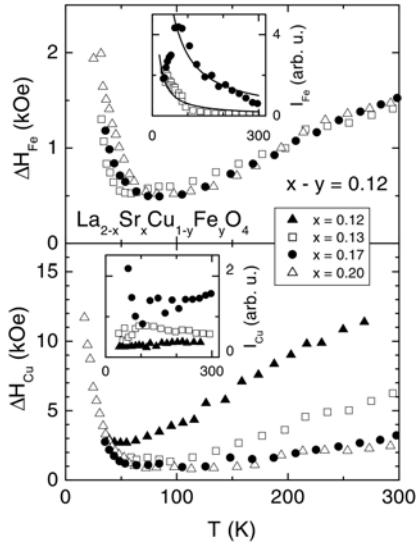


Fig. 1. Typical ESR spectrum as observed in  $\text{La}_{2-x}\text{Sr}_x\text{Cu}_{1-y}\text{Fe}_y\text{O}_4$ . The fit by two resonance lines is discussed in the text

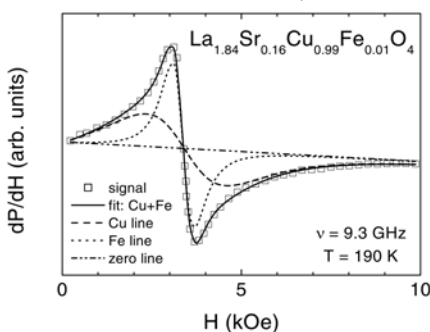
$g = 2$ , but with different linewidths  $\Delta H_1$  and  $\Delta H_2$  (here we use the full width at half maximum – FWHM – linewidth) for an appropriate fit of the ESR spectra:

$$P(H) \propto \sum_{i=1,2} \frac{\Delta H_i / 2 + \alpha(H - H_i)}{(H - H_i)^2 + (\Delta H_i / 2)^2} + \frac{\Delta H_i / 2 + \alpha(H + H_i)}{(H + H_i)^2 + (\Delta H_i / 2)^2}. \quad (1)$$

Due to the large linewidth we have to take into account both circular components ( $\pm H_i$ ) of each resonance. Although we use powdered samples, the skin effect can give rise to small contributions ( $\alpha \ll 1$ ) of dispersion to the absorption signal [14].

Fig. 1 shows such a typical ESR spectrum. The center of the signal is strongly disturbed by the well-known narrow Cu-oxygen-hole resonance [23]. We could minimize this spurious signal by a very careful sample preparation, but nevertheless, it was always observable. That is why we ignored the central part of the line for the fitting procedure. The remaining spectrum consists of a narrower line (dotted), which we will identify with the iron signal, and a broader resonance (dash line), which will turn out to originate from the Cu-spin system.

Fig. 2 gives an overview of the results obtained within a series of samples with a constant hole concentration and enables us to assign the two resonance lines unambiguously to Fe and Cu. In the lower frame the linewidth of the broader line is depicted. This broad signal is visible even in the sample without iron doping. Besides an upturn to low temperatures all data increase linearly with increasing temperature above 100 K, but the slope strongly decreases with increasing iron content  $y$  and remains constant for  $y \geq 0.05$ . The inset shows the corresponding intensities, which have been obtained as  $I \propto A\Delta H^2$ , where  $A$  denotes the amplitude of the derivative  $dP/dH$ . The skin effect can be neglected



here, because the dispersion contribution is always found to be  $\alpha \ll 1$ , i.e. the skin depth is large compared to the grain size. The intensities, which represent the local spin susceptibilities, all are approximately temperature independent above 60 K, (the intensities of the sample with  $y = 0.08$  have been omitted because of strong scattering of the data). Such a Pauli-like spin susceptibility

Fig. 2. Temperature dependence of linewidth and intensity (insets) for the resonance lines of iron (upper frame) and copper (lower frame) for a set of  $\text{La}_{2-x}\text{Sr}_x\text{Cu}_{1-y}\text{Fe}_y\text{O}_4$  with constant hole concentration  $p = x - y$ . The solid lines in the upper inset indicate Curie laws of the Fe intensities

Fig. 3. Temperature dependence of the copper linewidth for two sets of  $\text{La}_{2-x}\text{Sr}_x\text{Cu}_{1-y}\text{Fe}_y\text{O}_4$  with 1% Fe (upper frame) and 5% Fe (lower frame). The lines are drawn to guide the eye

has also been observed in  $\text{La}_{2-x}\text{Sr}_x\text{CuO}_4$  single crystals and has been explained as intrinsic Cu-ESR line, where a three-spin magnetic polaron in the  $\text{CuO}_2$  plane is regarded as the active ESR center [7,8]. In addition, the temperature dependence of the linewidth observed in the undoped polycrystal is – although shifted to higher values – in satisfactory agreement with the linewidth of the single crystal as well. Hence, we can assign the broad component of the ESR spectra to the intrinsic Cu signal.

The upper frame of Fig. 2 shows the same quantities for the narrower line, which is only present in the iron doped samples. Qualitatively, the temperature dependence is similar to that observed for the Cu signal, but the data nearly coincide for all values of  $y$ . This is a strong hint that for iron the hole concentration  $p$  is the decisive parameter, as will be discussed in detail below. The intensities, shown in the inset, follow quite well a Curie behavior indicated by the solid lines. Such a spin susceptibility is expected for localized magnetic impurities and, therefore, clearly identifies the Fe spins as the corresponding magnetic centers. The suppression of the intensity, which is observed below 80 K for higher Fe doping and which is accompanied by an increase of the Cu intensity, probably results from strong antiferromagnetic correlations with the surrounding Cu spins.

#### 4.2. Cu and Fe linewidth

Having identified the magnetic centers of the two ESR lines in  $\text{La}_{2-x}\text{Sr}_x\text{Cu}_{1-y}\text{Fe}_y\text{O}_4$  we turn now to the detailed investigation of the linewidth dependence on the composition parameters  $x$  and  $y$ . Figs. 3 and 4 summarize the results obtained for 1%- and 5%-Fe doped samples in the full Sr-concentration range under consideration for the Cu resonance as well as for the Fe resonance. In general, all data show a similar topology with a monotonous increase to high temperatures, a strong broadening to low temperatures, and a minimum in between.

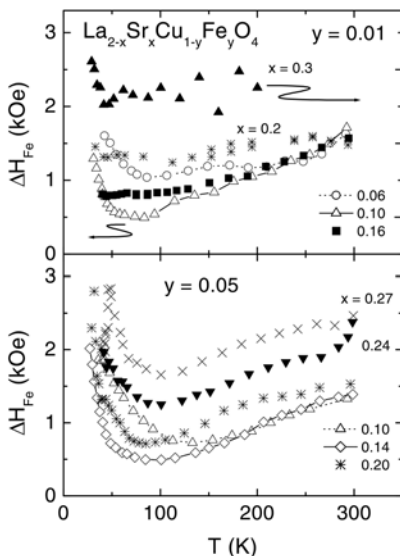
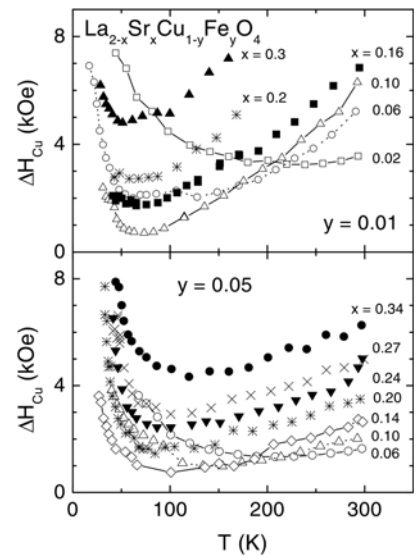


Fig. 4. Temperature dependence of the copper linewidth for two sets of  $\text{La}_{2-x}\text{Sr}_x\text{Cu}_{1-y}\text{Fe}_y\text{O}_4$  with 1% Fe (upper frame) and 5% Fe (lower frame). The lines are drawn to guide the eye. The right-hand axis of the upper frame is valid

Starting with the copper resonance in samples of 1% Fe doping, which is shown in the upper frame of Fig. 3, its temperature dependence is qualitatively comparable to that observed in both poly- and single crystals of the iron-free compounds [7,8]. With increasing Sr concentration  $x$  the slope  $b_{\text{Cu}}$  of the linear high-temperature regime increases up to  $b_{\text{Cu}} \approx 28$  Oe/K at  $x = 0.1$  (as compared to  $b_{\text{Cu}}(x = 0.1) \approx 40$  Oe/K for the iron-free sample) and remains nearly unchanged for higher  $x$ . At the same time, all data for  $x > 0.1$  exhibit a parallel shift to higher linewidth values, which increases with increasing Sr concentration. The iron resonance of the 1% Fe-doped series, which is shown in the upper frame of Fig. 4, first also evolves a linear increase at high temperatures of about  $b_{\text{Fe}} \approx 6$  Oe/K for  $x = 0.1$ . But with further increasing Sr concentration the slope is gradually suppressed and vanishes completely at  $x = 0.3$ , whereas the all-over value of the linewidth increases strongly.

Now we focus on the series with 5% Fe doping. Again the Cu resonance, shown in the lower frame of Fig. 3, evolves a linear high-temperature regime with increasing Sr concentration, but its slope remains at  $b_{\text{Cu}} \approx 11$  Oe/K for  $x \geq 0.14$ . Like in the case of 1% Fe doping all data for  $x \geq 0.14$  reveal the increasing parallel shift with increasing  $x$ . The Fe-linewidth obtained for  $y = 0.05$  is depicted in the lower frame of Fig. 4. Its behavior is now quite similar to that of the Cu resonance, but the absolute values of the linewidth are

about a factor of 2 smaller than for the copper signal.

For higher Fe concentrations the linewidths of Fe and Cu signal are fully correlated above  $T \approx 30$  K, as one can see for example in Fig. 5 for  $\text{La}_{1.8}\text{Sr}_{0.2}\text{Cu}_{0.9}\text{Fe}_{0.1}\text{O}_4$ . For  $30 < T < 130$  K the logarithmic plot of  $\Delta H_{\text{Cu}}$  and

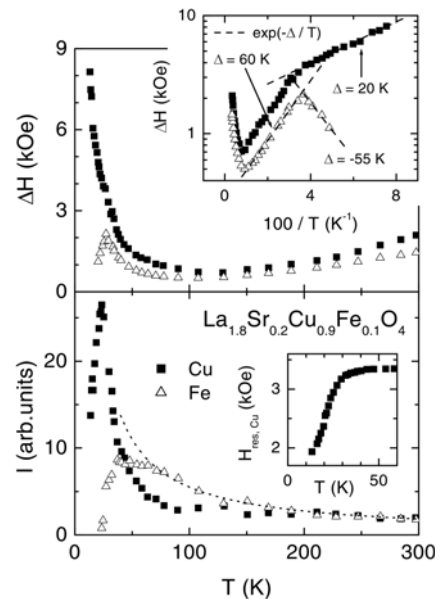


Fig. 5. Temperature dependence of Fe and Cu linewidth (upper frame, inset:  $\Delta H$  as function of inverse temperature) and Fe and Cu intensity (lower frame) in  $\text{La}_{1.8}\text{Sr}_{0.2}\text{Cu}_{0.9}\text{Fe}_{0.1}\text{O}_4$ . The dotted line indicates a Curie law for the Fe intensity. Inset: low-temperature resonance field for the Cu signal

$\Delta H_{\text{Fe}}$  versus the inverse temperature reveals an exponential dependence  $\exp(-\Delta/T)$  with  $\Delta \approx 60$  K for both quantities. Below 29 the Cu linewidth increases further exponentially with  $\Delta \approx 20$  K, whereas the Fe linewidth decreases with approximately the same slope in logarithmic representation like above 29 K, but with negative sign. At the same time the Cu-resonance field strongly shifts to lower fields with decreasing temperature down to 2 kOe at 14 K, where the signal becomes undetectable. At the temperature, where the correlation breaks, the Cu intensity exhibits a pronounced peak. The Fe intensity follows a Curie-law at high temperatures but reveals a broad maximum around 50 K and vanishes at about 20 K, probably due to the antiferromagnetic coupling to the Cu neighbors.

#### 4.3. Analysis

In metallic compounds with localized magnetic moments the probing spin can relax both via the mobile charge carriers and via the spin fluctuations of the localized moments. The first process is the well-known Korringa relaxation giving rise to a linear temperature dependence [14]

$$\Delta H_K = bT \quad (2)$$

with the slope  $b \propto N^2(E_F)$  proportional to the squared density of states  $N$  at the Fermi energy ( $E_F$ ). The second process, which is mediated via super-exchange or RKKY-like interactions, contributes as [25]

$$\Delta H_f \propto \frac{T}{\omega} \chi_f''(\mathbf{Q}, \omega) \quad (3)$$

with the imaginary part of the dynamic susceptibility  $\chi_f''(\mathbf{Q}, \omega)$  of the fluctuating spin system. Neglecting the dependence on the momentum transfer  $\mathbf{Q}$  and using a purely relaxational ansatz the frequency dependence can be approximated as

$$\chi_f''(\omega) = \frac{\omega\tau}{1 + \omega^2\tau^2} \chi_0 \quad (4)$$

with the spin-correlation time  $\tau$  and the static spin susceptibility  $\chi_0$ . For correlation times  $\tau$  short as compared to the inverse probing frequency  $1/\omega$ , i. e.  $\omega\tau \ll 1$  this results in

$$\Delta H_f \propto T\chi_0\tau \quad (5)$$

which yields a measure for the spin-correlation time, as the static susceptibility is known.

Based on these fundamental relations, we analyze the complex spin dynamics in iron doped  $\text{La}_{2-x}\text{Sr}_x\text{CuO}_4$ . The fluctuating system ( $\chi_f(\mathbf{Q}, \omega)$ ) of localized moments has to be identified with the entire  $\text{Cu}^{2+}$ -spin system, which cannot be detected directly by ESR experiments because of the relaxation processes being too fast [6]. The mobile charge carriers are the holes induced by  $\text{Sr}^{2+}$  substitution for  $\text{La}^{3+}$ . Beside the  $\text{Fe}^{3+}$  ESR probes there are the Cu-spin polarons with properties strongly related to the entire Cu system. The polaron signal has been discussed in detail [8,27] for the pure compound, where it behaves very similar to the 1% Fe-doped samples (cf. upper frame in Fig. 3). Although several reasons for the high-temperature behavior of the linewidth are under debate, it seems reasonable to assume a Korringa-like relaxation of the polarons to the mobile holes as the dominant mechanism. This is supported by the evident similarity of the concentration dependence of the square-root of the high-temperature slope in  $\Delta H(T)$  and the averaged electronic density of states at the Fermi energy determined by optical reflectivity [28]. This mechanism is also consistent with the additional influence of the iron, as we will explain immediately.

Fig. 6 summarizes the high-temperature behavior of both Cu and Fe linewidth obtained at room temperature as a function of the hole concentration  $p = x - y$ . For iron the linewidth shows a monotonous increase with increasing hole concentration, independent on the specific Sr:Fe ratio (cf. also Fig. 2). Interestingly the slope of this increase exhibits an abrupt change near the optimal doping concentration ( $p = 0.15$ ), where the highest  $T_c$  is reached for  $y = 0$ . Taking into account that at high temperatures the Fe linewidth increases approximately linear with temperature in most of the samples under investigation, at first glance the  $T$ -linear increase of  $\Delta H_{\text{Fe}}$  could be interpreted as Korringa broadening via scattering at the charge carriers, which should be the same for all samples with the same charge-carrier concentration  $p$ . The copper linewidth also monotonously increases with  $p$  at a given iron content  $y$ , as indicated by the open triangles ( $y = 0.01$ ) and circles ( $y = 0.05$ ), but it exhibits an additional strong pronounced dependence on  $y$  itself, as one can see from the series of constant Sr contents ( $x = 0.1, 0.2, \text{ and } 0.3$ ), which are connected via the dash lines. The strong decrease

Fig. 6. Dependence of the room-temperature linewidth on hole concentration  $p = x - y$  for  $\text{La}_{2-x}\text{Sr}_x\text{Cu}_{1-y}\text{Fe}_y\text{O}_4$  for the copper signal (upper frame - dotted lines connect data points of  $y = \text{const}$ , dash lines connect series of  $x = \text{const}$ ) and the iron signal (lower frame - solid lines indicate the different slope below and above  $p = 0.15$ )

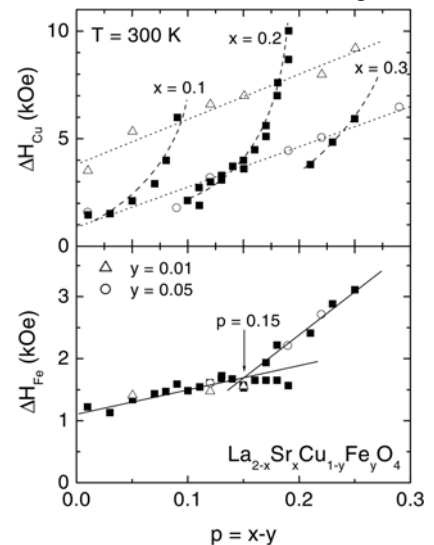


Fig. 7. Temperature dependence of the Fe linewidth (upper frame) Cu intensity (middle frame) and inverse spin fluctuation time (lower frame) for  $\text{La}_{2-x}\text{Sr}_x\text{Cu}_{1-y}\text{Fe}_y\text{O}_4$

of  $\Delta H_{\text{Cu}}$ , in spite of constant  $p$  but with increasing  $y$ , shows that the Fe ions obviously provide a reduction of the number of mobile charge carriers. In particular at the borderline  $x = 0.1/0.2$  for  $p = 0.1$  or at  $x = 0.2/0.3$  for  $p = 0.2$ , there is always a prominent broadening on the side of low Fe concentration, whereas on the side of high Fe concentration the lines are much narrower. Hence, we conclude that the  $\text{Fe}^{3+}$  ions act as localization centers for the mobile charge carriers, i.e. the number of those is reduced with larger Fe concentration. This assumption is also supported by the Cu-linewidth data in Fig. 2, where the samples with the higher  $y$ -values show the smaller Korringa slope at high temperatures. It is important to note that no such localization effects are visible in  $\Delta H_{\text{Fe}}$ . It seems that the charge carriers (holes in the oxygen  $p$ -orbitals) are hardly scattered by the  $\text{Fe}^{3+}$  ions. The evolution of  $\Delta H_{\text{Fe}}(y = 0.01)$  with increasing  $x$  reveals just the opposite behavior than  $\Delta H_{\text{Cu}}$ , i.e. the Korringa-like increase visible for  $x = 0.1$  becomes completely suppressed up to  $x = 0.3$ , where a large temperature-independent linewidth is observed. This is in contradiction to the Korringa relaxation at all, as we know that the electronic density of states is approximately constant for  $0.1 < x < 0.3$  [28]. Therefore the Korringa process can be ruled out for the line broadening of the Fe resonance, which is consistent with the resistivity results described above, where the conductivity was only dependent on  $p$  but not affected by the presence of  $\text{Fe}^{3+}$  as additional scattering center.

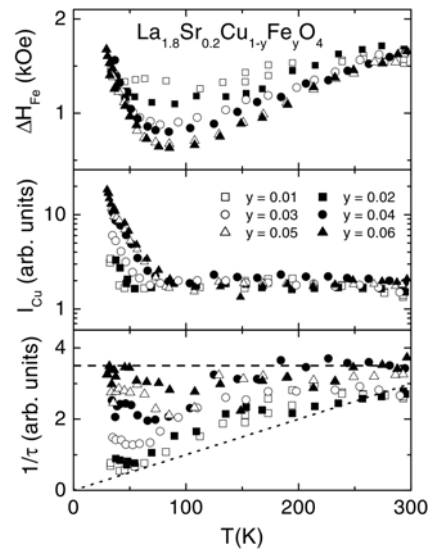
Without Korringa scattering, the relaxation of the iron spins should be fully determined by the dynamic susceptibility of the copper-spin system. Hence, we try to evaluate the linewidth data in terms of Eq. 5 now. The static copper susceptibility is approximately constant in temperature. Then a linear increase of  $\Delta H_{\text{Fe}}(T)$  with increasing temperature indicates a temperature-independent spin-correlation time  $\tau = \text{const}$ , whereas a temperature-independent linewidth yields a  $\tau(T) \propto 1/T$  behavior. In the latter case, the spin fluctuations follow the so called  $\omega/T$  scaling, which has been observed for  $\text{La}_{2-x}\text{Sr}_x\text{CuO}_4$  by neutron-scattering experiments e.g. for  $x = 0.02$  [30],  $x = 0.04$  [29],  $x = 0.07$  [31], and  $x = 0.14$  [32].

Regarding the high-temperature behavior of  $\Delta H_{\text{Fe}}(T)$  for  $y = 0.01$  in the upper frame of Fig. 4, the temperature-independent linewidth, which indicates  $\omega/T$  scaling of the copper-spin fluctuations, is approached above  $x > 0.1$ . For lower Sr concentrations, the linear high-temperature increase indicates temperature-independent spin fluctuations, which seem to be in contradiction to the neutron-scattering results. However, this can be understood in terms of the localization effect: The  $\text{Fe}^{3+}$  ion repels the holes and, therefore, reduces the coupling of the holes with the neighboring  $\text{Cu}^{2+}$  spins. The missing interaction with the charge carriers obviously yields a temperature-independent spin-correlation time of these copper spins. As the iron spin primarily couples to its nearest copper neighbors, these fluctuations, which do not follow the  $\omega/T$  scaling, dominate its relaxation behavior at low Sr concentration  $x$ . With increasing  $x$  this localization effect for the copper spins, which surround the  $\text{Fe}^{3+}$  ion, is overcome by the increasing number of mobile holes, resulting in the temperature independent linewidth.

So far we can explain the asymptotic high-temperature behavior of the iron linewidth by the copper-spin fluctuations and localization of holes. Now we will extend our approach to the full temperature range, as the simultaneous observation of iron and copper resonance allows to extract the spin-correlation time  $\tau$  as a function of temperature. This has been done in Fig. 7 for  $\text{La}_{1.8}\text{Sr}_{0.2}\text{Cu}_{1-y}\text{Fe}_y\text{O}_4$  with  $0.01 \leq y \leq 0.06$ , which shows the iron linewidth  $\Delta H_{\text{Fe}}$  in the upper frame and the corresponding intensity  $I_{\text{Cu}}$  of the Cu-polaron signal in the middle frame. The inverse spin-correlation time, shown in the lower frame, was determined assuming  $I_{\text{Cu}}$  as proportional the spin susceptibility of the entire Cu system. This yields a very reasonable result. For low Fe concentration  $y$  we obtain an approximately linear dependence  $1/\tau \propto T$ , indicative for spin fluctuations following the  $\omega/T$  scaling, which gradually changes into the  $(1/\tau = \text{const})$  behavior with increasing  $y$ , when the localization becomes dominant.

This analysis shows that Eq. 5 even correctly describes the line broadening at low temperatures, where the Cu-intensity strongly increases. The increase of the Cu intensity can be understood from the ferromagnetic polarization of the Cu spins by the interaction with the holes [33]. The transition from itinerant to localized holes yields an amplification of the ferromagnetic polarization and hence of the local Cu susceptibility. The localization mechanism is further supported by the exponential temperature dependence of both Fe and Cu linewidth as indicated in Fig. 5. In pure  $\text{La}_2\text{CuO}_4$  the temperature dependence of the linewidth can be related to the exponential temperature dependence of the correlation length of the Cu-spin fluctuations [4]. However, this model fails for the Sr-doping regime of the metal-to-insulator transition, because here a temperature-independent correlation length was found by neutron-scattering experiments [29]. Considering the hole localization, the ferromagnetic polarization of the Cu spins is connected with the duration time, which the hole resides in a localized orbital. The thermal activation of the holes results in the exponential temperature dependence of the local Cu susceptibility and in turn of the linewidth of Fe and Cu-polaron signal.

The behavior below the peak in the Cu intensity at 29 K is difficult to interpret. Probably the peak can be identified with the transition into the spin-glass phase [17]. This is also supported by the strong shift of the Cu resonance below 29 K. Here the hopping motion of the holes freezes and only tunneling processes with lower activation



energy take place, resulting in the change of the slope in the logarithmic plot of the Cu linewidth. The Cu intensity reduces due to local antiferromagnetic order of the Cu spins. This opens a gap in the spin-fluctuation spectrum, which decouples the relaxation of the Fe signal resulting in the observed decrease of the Fe linewidth.

With a nearly symmetric shape in the  $1/T$  representation, the peak in the Fe linewidth reminds to the characteristics of a Bloembergen-Purcell-Pound (BPP) mechanism. From NMR experiments this is known to appear in the nuclear spin-lattice relaxation rate  $1/T_1$ , if the fluctuation rate slows down on lowering the temperature and, thereby, crosses the experimental frequency [34]. Indeed the BPP mechanism was suggested to explain the NMR-relaxation rate  $1/T_1$  of  $^{139}\text{La}$  in  $\text{La}_{1.67}\text{Eu}_{0.2}\text{Sr}_{0.13}\text{CuO}_4$ , which exhibits a slightly asymmetric peak near 9 K [35]. Additionally, a slowing down of the antiferromagnetic dynamics has been reported from  $\text{Gd}^{3+}$ -ESR experiments in  $\text{La}_{1.65}\text{Gd}_{0.01}\text{Eu}_{0.24}\text{Sr}_{0.1}\text{CuO}_4$ , where the fluctuation frequencies have been found to decrease from  $10^{12}$  Hz by three orders of magnitude below 50 K [36], i.e. the approximation used to derive Eq. 5 is not valid any more at lowest temperatures. More systematic ESR investigations at different probing frequencies and accompanying  $^{139}\text{La}$ -NMR measurements on the same samples are necessary to characterize the low-temperature behavior in detail.

## 5. Summary

By a careful analysis of the ESR line shape of  $\text{La}_{2-x}\text{Sr}_x\text{Cu}_{1-y}\text{Fe}_y\text{O}_{4-\delta}$  we could separate the Fe and the Cu resonances. There is no Korringa broadening in the Fe resonance. Its broadening in the temperature range  $80 \leq T \leq 300$  K is only caused by fluctuations in the Cu-bath. The Cu-bath exhibits two components of spin fluctuations - one with a temperature-dependent ( $\tau \propto 1/T$ ) and the other with a temperature-independent correlation time, where the second one characterizes the Cu spins in the direct neighborhood of the Fe spin. The addition of  $\text{Fe}^{3+}$  ions favors a localization of the charge carriers. The exchange between the Fe and the Cu system is obviously not strong enough to establish a bottleneck effect like in Mn-doped  $\text{La}_{2-x}\text{Sr}_x\text{CuO}_4$ . Normally, the ESR of  $3d$ -ions in metals is only observable in the bottleneck regime. It seems that  $\text{La}_{2-x}\text{Sr}_x\text{Cu}_{1-y}\text{Fe}_y\text{O}_4$  forms the first exception from this rule, probably due to the weak coupling with the charge carriers. From our investigations we infer that  $p = x - y$ , i.e. the number of charge carriers is a crucial parameter to compare the various experimental results.

## 6. Acknowledgments

We thank Prof. Dr. B. I. Kochelaev for many useful discussions. This work is supported by the German Bundesministerium für Bildung und Forschung under the contract No. VDI/EKM 13N6917 and by the Deutsche Forschungsgemeinschaft (DFG) via the Sonderforschungsbereich SFB 484 (Augsburg).

## References

1. G. Bednorz and K.A. Müller, *Z. Phys. B: Condens. Matter* **64**, 189 (1986).
2. M. Imada, A. Fujimori, and Y. Tokura, *Rev. Mod. Phys.* **70**, 1039 (1998).
3. T. Moriya and K. Ueda, *Rep. Prog. Phys.* **66**, 1299 (2003).
4. S. Chakravarty and R. Orbach, *Phys. Rev. Lett.* **64**, 224 (1990).
5. A.V. Lazuta, *Physica C* **181**, 127 (1991).
6. B.I. Kochelaev, *J. Supercond.* **12**, 53 (1999).
7. J. Sichelschmidt, B. Elschner, and A. Loidl, *Physica B* **230-232**, 841 (1997).
8. B.I. Kochelaev, J. Sichelschmidt, B. Elschner, W. Lemor, and A. Loidl, *Phys. Rev. Lett.* **79**, 4274 (1997).
9. J. Sichelschmidt, B. Elschner, A. Loidl, and K. Fischer, *Z. Phys. B: Condens. Matter* **93**, 407 (1994).
10. J. Sichelschmidt, B. Elschner, A. Loidl, and B. I. Kochelaev, *Phys. Rev. B* **51**, 9199 (1995).
11. B. Elschner and A. Loidl, in *Handbook of the Physics and Chemistry of Rare Earth*, edited by K. A. Gschneidner jr., L. Eyring, and M. B. Maple (Elsevier Science, Amsterdam, 2000), Vol. 30, p. 375.
12. B.I. Kochelaev, L. Kan, B. Elschner, S. Elschner, *Phys. Rev. B* **49**, 13106 (1994).
13. A. Shengelaya, H. Keller, K.A. Müller, B.I. Kochelaev, K. Conder, *Phys. Rev. B* **63**, 144513 (2001); *J. Supercond.* **13**, 955 (2000).
14. S.E. Barnes, *Adv. Phys.* **30**, 801 (1981).
15. A. Sienkiewicz, M.Z. Cieplak, G. Xiao, and C.L. Chien, *J. Less Common Metals* **164&165**, 870 (1990).
16. M. Coldea, *Physica C* **185-189**, 1197 (1991).
17. M.Z. Cieplak, A. Sienkiewicz, F. Mila, S. Guha, G. Xiao, J.Q. Xiao, and C.L. Chien, *Phys. Rev. B* **48**, 4019 (1993).
18. J. Arai, T. Nitta, and N. Mori, *Physica C* **235-240**, 1649 (1994).
19. A.D. Shengelaya, J. Olejniczak, and H. Drulis, *Physica C* **233**, 124 (1994).
20. J. Arai, K. Kojima, and N. Mori, *J. Low Temp. Phys.* **105**, 455 (1996).
21. I. Felner, J. Gersten, A. Minakov, M. Merzlyakov, and Yu. Bugoslavsky, *Physica C* **261**, 207 (1996).
22. A.D. Shengelaya, J. Olejniczak, H. Drulis, and N.M. Suleimanov, *Solid State Commun.* **99**, 779 (1996).
23. J. Stankowsky, W. Hilzner, J. Baszynski, B. Czyzk, and L. Szczepanka, *Solid State Commun.* **77**, 125 (1991).
24. H. Takagi, T. Ido, S. Ishibashi, M. Uota, S. Uchida, and Y. Tokura, *Phys. Rev. B* **40**, 2254 (1989).
25. M. Coldea, H. Schäffer, V. Weissenberger, and B. Elschner, *Z. Phys. B: Condens. Matter* **68**, 25 (1987).
26. G. Kruschel, Ph.D.Thesis, TU Darmstadt (1993).
27. J. Sichelschmidt, Ph.D.Thesis, TU Darmstadt (1997).
28. S. Uchida, T. Ido, H. Takagi, T. Arima, Y. Tokura, and S. Tajima, *Phys. Rev. B* **43**, 7942 (1991).

29. B. Keimer, N. Belk, R.J. Birgenau, A. Cassanho, C.Y. Chen, M. Gerven, M.A. Kastner, A. Aharony, Y. Endoh, R.W. Erwin, and G. Shirane, *Phys. Rev. B* **46**, 14034 (1992).
30. M. Matsuda, R.J. Birgenau, Y. Endoh, Y. Hidaka, M.A. Kastner, K. Nakajima, G. Shirane, T.R. Thurston, and K. Yamada, *J. Phys. Soc. Jpn.* **62**, 1702 (1993).
31. H. Hiraka, Y. Endoh, M. Fujita, Y.S. Lee, J. Kulda, A. Ivanov, and R.J. Birgenau, *J. Phys. Soc. Jpn.* **70**, 853 (2001).
32. G. Aeppli, T.E. Mason, S.M. Hayden, H.A. Mook, and J. Kulda, *Science* **278**, 1997 (1432).
33. A. Aharony, R.J. Birgenau, A. Coniglio, M.A. Kastner, and H.E. Stanley, *Phys. Rev. Lett.* **60**, 1330 (1988).
34. N. Bloembergen, E.M. Purcell, and R.V. Pound, *Phys. Rev.* **73**, 679 (1948).
35. B.J. Suh, P.C. Hammel, M. Hücker, B. Büchner, U. Ammerahl, and A. Revcolevschi, *Phys. Rev. B* **61**, 9265 (2000).
36. V. Kataev, B. Rameev, B. Büchner, M. Hücker, and R. Borowski, *Phys. Rev. B* **55**, 3394 (1997).